Diffusional Motion of a Particle Translocating through a Nanopore

Wen-Jie Lan and Henry S. White*

Department of Chemistry, University of Utah, 315 S 1400 E, Salt Lake City, Utah 84112, United States

ABSTRACT

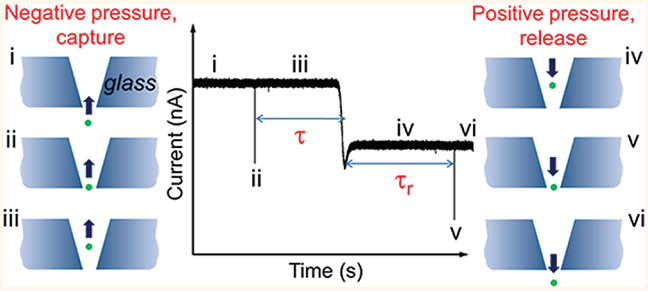

The influence of diffusional motion on the capture and release of individual nanoparticles as they are driven through a conical-shaped glass nanopore membrane (GNM) by pressure-induced flow is reported. In these experiments, one to several hundred particles are driven through the orifice of the nanopore. Following the initial translocation, the pressure is reversed and the particles are driven through the GNM orifice in the reverse direction. The resistive-pulse technique is used to monitor the temporal sequence of particle capture and release translocations. The size of the particles (120−160 nm) and the direction of translocation can be determined from the pulse amplitude and shape. The stochastic influence of diffusion on particle trajectories has been investigated, including instantaneous transfer rate, release probability, and cumulative release success rate. We demonstrate that the sequence of particle translocations in the capture step (*a*, *b*, *c*... where the letters represent different particles) is largely preserved and can be read out by resistive-pulse signature during the release translocations (...*c*, *b*, *a*). The observed stochastic events are in good agreement with a convective diffusion model of particle trajectory within the confined geometry of the nanopore. The pressure-reversal technique opens new avenues for chemical analysis of particles using resistive-pulse methods.

KEYWORDS: nanopore · resistive pulse · capture and release · diffusion · Coulter counter

We report a pressure-reversal resistive-pulse method to capture and release nanoparticles using a conical-shaped nanopore. The objective of this study is to probe the influence of thermal diffusion on particle trajectories during translocation through a nanopore. The resistive-pulse technique was invented by W. H. Coulter in 1953 as a means of counting and sizing particles in a conducting fluid.[1] Particles in an electrolyte solution are driven through an orifice separating two Ag/AgCl electrodes, and the current between the electrodes is momentarily interrupted when a particle passes through the orifice.[2] Typically, the rate of particle translocation is used to determine the solution particle concentration, while the duration time and the peak height are analyzed to determine the particle size and shape. During the past decade, the development of both synthetic[3−7] and biological nanopores[8−13] has attracted significant attention due to the application of the resistive-pulse method in analyses of nanoparticles[14−18] and molecules.[19−21]

A pressure-reversal technique using cylindrical micropores (3−30 μm in diameter) was first reported by Berge, Feder, and Jossang in 1989.[22,23] A trigger signal from the particle translocation event was used to activate two miniature solenoid valves to control the direction of pressure-driven flow. Capture and release translocations were demonstrated for particles, bacteria, and dissolving air bubbles. More recently, Gershow and Golovchenko studied the forward and reverse translocation of a single DNA molecule through a solid-state nanopore by reversing the transmembrane potential direction after the initial translocation, and they analyzed the probability of observing the release translocation using a drift-diffusion physical model.[24,25] Meller,[26] Hibbs,[27] and co-workers also applied similar voltage switching methods to investigate diffusional motion of DNA in a protein channel.

The experiment reported herein is depicted in Figure 1. Pressure applied across a glass nanopore membrane (GNM) is controlled using a gastight syringe. The GNM, schematically shown in Figure 2, is a single conical nanopore embedded in a thin glass membrane (50−100 μm), with the smaller-radius orifice facing the external solution. The GNM is fabricated using simple benchtop methods previously described by our laboratory.[28−31] A three-part pressure waveform (Figure 1a) drives an individual particle or

* Address correspondence to white@chem.utah.edu.

Received for review December 6, 2011 and accepted January 2, 2012.

Published online January 02, 2012
10.1021/nn2047636

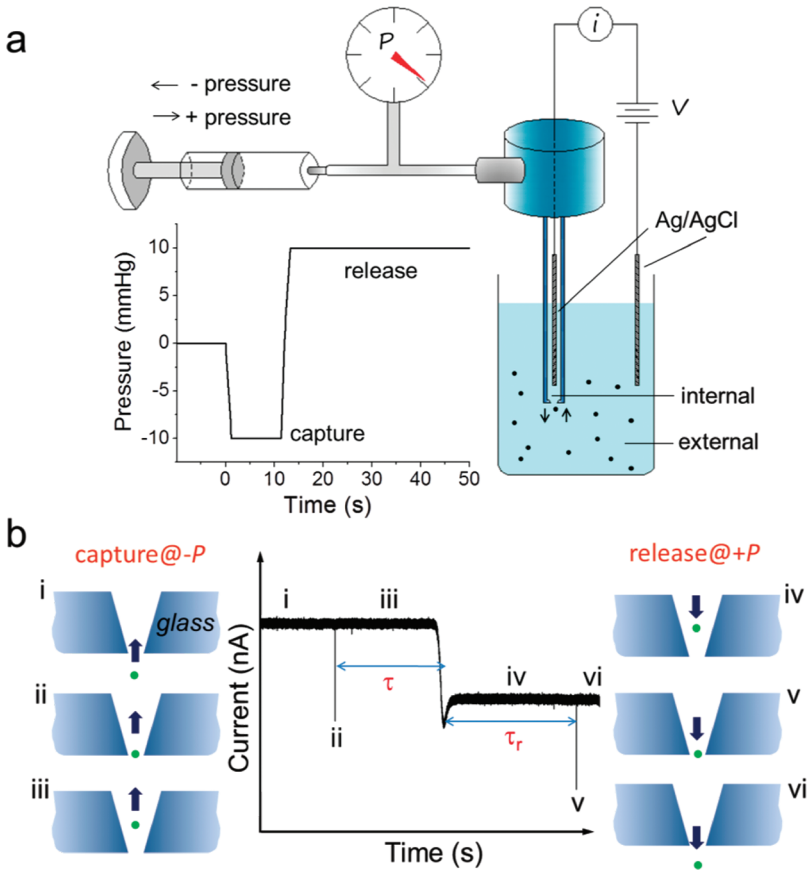

Figure 1. (a) Schematic illustration of glass nanopore membrane (GNM), and particle capture and release method using a three-part pressure waveform. (b) Schematic of the particle translocation and resulting *i*−*t* recording. The arrows represent the direction of particle movement. (i) The particle moves toward the pore orifice from the external solution after the initial application of −*P*. (ii) The particle translocates through the pore, generating a pulse in the *i*−*t* recording. (iii) The particle continues traveling into the pore interior under pressure-driven flow. (iv) The pressure is reversed (+*P*) at τ, and the particle moves toward the pore. (v) The particle translocates through the pore at τ_r, generating a second resistive pulse and (vi) returns to the external solution.

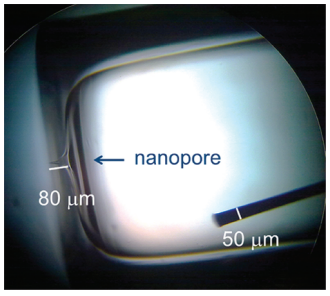

Figure 2. Optical microscopy image of the GNM (side view) used in recording the translocation data presented in the main text. A 50 μm diameter W rod was inserted into the capillary for length calibration (bottom right). The GNM thickness was measured to be ~80 μm.

a large group of particles back and forth through the GNM orifice. Upon application of a negative pressure inside the GNM (−*P*) (Figure 1b), the particle is initially driven from the external solution through the pore orifice, generating a pulse in the *i*−*t* recording. After a preset period of time, τ, following the initial translocation, the pressure is switched to a positive pressure (+*P*) and the same particle translocates through the pore orifice in the opposite direction, generating a current pulse at release time τ_r. In the absence of any stochastic influences, τ_r should equal τ if the initial (−*P*) and reversal (+*P*) pressure are identical. This assumes that the nanoparticle's motion is determined by the velocity of the solution through the nanopore, which is proportional to the applied pressure. A consequence of this equivalence of τ_r and τ is that, when multiple particles are driven through the orifice, the order in which they retranslocate, upon the pressure reversal, is reversed to the order of the initial translocation. That is, the time sequence of particle translocations in the capture step (τ_a, τ_b, τ_c ... where the letters represent different particles) is preserved and can be read out by resistive pulses during the release translocations (...τ_{rc}, τ_{rb}, τ_{ra}). In this article, we show that this sequence information is largely preserved, but that diffusional motion of the particle introduces a stochastic broadening of the particle location and, thus, τ_r.

RESULTS AND DISCUSSION

Capture and Release of 120 and 160 nm Radius Particles in a Mixed Particle Solution. We first investigated particle translocation using a 210 nm radius GNM that joined

two reservoirs of aqueous 0.1 M KCl maintained at pH 7.4 by a 10 mM K_2HPO_4/KH_2PO_4 buffer. A mixture of nonfunctionalized 120 nm and −COOH modified 160 nm radius particles was added to the external solution and a 200 mV potential applied across the GNM (internal *vs* external solution). The top panel in Figure 3 shows a typical *i*−*t* recording for the capture and release of three particles recorded over an 8 s interval. The particles were first driven through the pore from external solution and detected as they passed through the small orifice by a momentary blockage of the ionic current. Three resistive pulses are observed, denoted as *a*, *b*, and *c*. The size of the particles can be unequivocally assigned by the resistive-pulse heights, as determined in experiments using only 120 nm radius particles or only 160 nm radius particles. Thus, the smaller pulse *a* corresponds to the 120 nm radius particle, while the larger pulses *b* and *c* correspond to two 160 nm radius particles.

Upon translocation, the three particles were driven into the nanopore by pressure-driven flow for a time period. The pressure was then reversed to bring the same particles back through the GNM orifice, yielding pulses *c*′, *b*′, and *a*′, where *c*′ and *b*′ correspond to the two 160 nm radius particles and pulse *a*′ corresponds to the smaller 120 nm radius particle. This reverse order of particle translocation is typical of the capture and release experiment; the first particle to be captured is typically the last particle to be released. However, as shown below, diffusional broadening of the particle location after it is captured results in stochastic release times, which can scramble the sequence information.

Spherical particle translocation through a conical pore results in an asymmetric triangular pulse in the *i*−*t* recording as previously detailed[32,33] and demonstrated in the enlarged *i*−*t* curves in Figure 3 for capture/release pulse pairs *a*/*a*′ and *b*/*b*′. For capture translocation, the current initially decreases steeply to a minimum value, and then slowly increases back to the baseline (pulses *a* and *b*). In contrast, the release pulse shape is the mirror image of the capture pulse shape; a slow current decrease followed by a sharp increase, as shown for pulses *a*′ and *b*′. Thus, the particle translocation direction can be readily distinguished from *i*−*t* recordings based on the peak shape.

In addition to pressure-driven solution flow, particle motion in these experiments may be potentially influenced by diffusion, migration, electrostatic interaction with the nanopore surface charge, and electroosmotic flow (EOF). Since the nanopore has been silanized to reduce the GNM surface charge, and the experiments were performed in a relatively high electrolyte concentration (0.1 M), we assume that the electrostatic repulsion and EOF have a negligible influence on the particle's motion. The ζ-potential of the nonfunctionalized 120 nm radius particles dispersed in a 0.1 M KCl

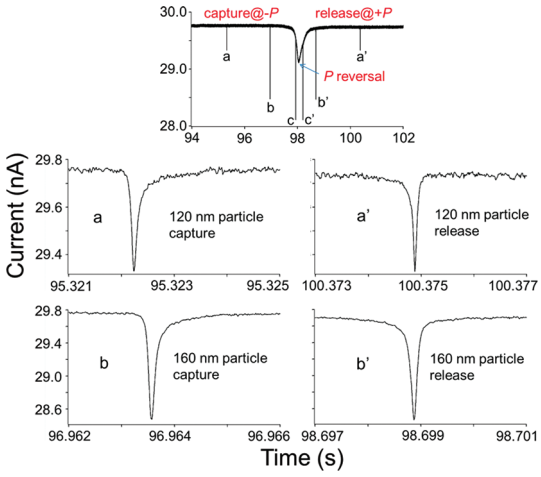

Figure 3. Recordings of *i*−*t* corresponding to the capture and release of 120 and 160 nm radius nanoparticles using a 210 nm radius GNM in a 0.1 M KCl solution (pH 7.4) at *P* = −5 mmHg (capture) and *P* = +5 mmHg (release). Pulses denoted by (a), (b), and (c) correspond to translocation of a 120 nm radius and two 160 nm radius particles, respectively, from the bulk solution into the GNM ("capture"). Pulses denoted by (a′), (b′), and (c′) correspond to translocation of the same 120 and 160 nm radius particles from the GNM back into the bulk solution ("release"). V_{app}: 200 mV internal *vs* external solution. Expanded *i*−*t* traces are shown for pulses (a), (a′), (b), and (b′).

solution (pH 7.4) was measured to be less than −2 mV, which we assume is sufficiently small that electrophoretic transport can be ignored. All following experiments were performed with these nonfunctionalized 120 nm radius particles.

In the absence of particle diffusion, the capture time, τ, and release time, τ_r, for pressure-driven flow should be identical. Due to diffusion, τ and τ_r are not equal and the sequence of particle release is not necessarily the reverse of the order of particle capture. A measure of the distance that a particle diffuses, δ, along the direction of the nanopore's central axis, during the time period, *t*, following the initial capture, can be estimated using the Einstein relationship[34−36]

$$\delta^2 = 2Dt \quad (1)$$

The particle diffusivity, *D*, is estimated by the Stokes−Einstein equation

$$D = \frac{k_B T}{6\pi\eta r} \quad (2)$$

where k_B is the Boltzmann constant, *T* is the absolute temperature, η is the viscosity of the solution, and *r* is the particle radius. For a 120 nm radius particle, *D* is 2.0×10^{-12} m^2/s and δ was computed to be 4.5 μm in a 5 s duration (corresponding approximately to the time between capture and release of the 120 nm radius particle (pulses *a* and a′) in Figure 3). The 120 nm radius particle is estimated to travel, by pressure-driven flow, a distance of ∼50 μm from the pore orifice through the

nanopore in this 5 s duration, assuming that the particle travels uniformly with the fluid along the pore axis. Thus, diffusion is expected to lead to a ~10% variation in τ_r following the pressure reversal. Note here that our estimation only takes into account one-dimensional diffusion. The actual three-dimensional particle diffusion within the nanopore may cause more variation into τ_r. A detailed simulation of the particle trajectory is described in the following sections.

Capture and Release of Multiple 120 nm Radius Particles. Experiments were carried out in a concentrated PS particle solution (~10^{10} particles/mL) in order to capture and release large numbers of nanoparticles over a short period of time. Negative pressure was first applied for a predetermined time period (~12 s; see Figure 4a), resulting in translocation of 440 particles through the GNM. The pressure was then reversed and maintained. The particles, having just passed through the GNM, now travel in the opposite direction through the GNM. Following pressure reversal at ~12 s, 441 particles translocated back through nanopore over a ~80 s period. The small discrepancy between the number of particles captured and released (generally <2%) is likely due to impurities or an undercounting of events in the capture or release stage due to coincident particle translocation.

Figure 4b shows the rate of particle translocation for the data presented in Figure 4a at different times during capture and release. Each data point represents the translocation rate in a 1 s interval centered about the corresponding time. The error bars represent the precision (1σ) from repeating the measurement six times. The bold black lines represent the predictions of the finite-element simulation, which will be discussed below. For capture translocations, the rate increased during the first 1 s following the pressure application and then remained constant at ~33 events·s^{-1} (the slow increase results from manual application of the pressure, which requires ~1 s). The relatively large error bars for the experimental translocation rates are due to stochastic fluctuations and the small bin size (1 s). After the pressure is reversed, the particle release transfer rate is constant and equal to the capture rate (~33 events·s^{-1}), and then slowly decreases over time as all of the particles are released.

Finite-Element Simulations. A diffusion–convection model was used to quantitatively predict the stochastic instantaneous particle translocation event rate, using the Ergodic principle to relate observations of discrete particle translocation events to calculations based on continuum analytical expressions. In our continuum-based simulations, the finite size of the particle is not considered. To simplify the model, the 0.1 M KCl solution was considered as incompressible, and migration and electroosmosis were ignored. A physical description of the pressure-driven flow in a pore begins

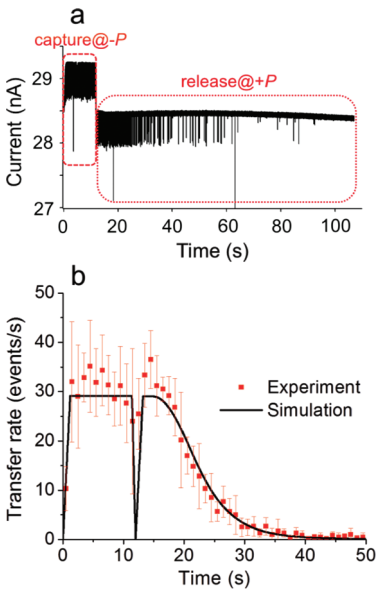

Figure 4. (a) Recording of i–t for the capture and release of 120 nm radius particles (GNM size: 210 nm radius, 1.3 × 10^{10} particles/mL, V_{app}: 200 mV internal *vs* external). A −10 mmHg pressure was applied to drive the particles through the pore (0 to ~12 s). The pressure was reversed to 10 mmHg at ~12 s and maintained until ~110 s to drive the particles inside the pore back to the external solution. (b) Instantaneous translocation rates for the particle capture and release experiments (±10 mmHg pressures for the data in part a). Each red point represents the rate at which particles enter the pore within a 1 s time interval (for example, the point at 0.5 s represents the rate within the interval 0 and 1 s and is average of six repetitive experiments analogous to that shown in part a). The bold black line represents the transfer rate predicted by finite-element simulations.

with the Navier–Stokes equation.

$$\mathbf{u}\nabla\mathbf{u} = \frac{1}{\rho}(-\nabla P + \eta\nabla^2\mathbf{u}) \quad (3)$$

In eq 3, **u** is the local position-dependent fluid velocity, ρ and η are the density and viscosity of the fluid, respectively, and P is the pressure.

The particle distribution and flux inside the pore were modeled by the Nernst–Planck equation, assuming electroneutrality and ignoring particle migration.

$$\mathbf{J} = -D\nabla c + c\mathbf{u} \quad (4)$$

In eq 4, **J** and c are, respectively, the flux and concentration of the particles. The two terms on the right-hand side represent diffusion and the pressure-driven convection. The finite-element method was utilized to solve the coupled equations, details of which are presented in the Supporting Information file. The glass surface of the nanopore was defined as an uncharged and insulating boundary. Input parameters were chosen to reflect a 0.1 M KCl solution (T = 298 K, ρ = 10^3 kg·m^{-3}, and η = 8.9 × 10^{-4} Pa·s).

The orifice radius and length of the GNM were set to 210 nm and 80 μm (Figure SI1), respectively

(corresponding to actual size of the GNM, Figure 2). To approximate the semi-infinite volume of the solution far away from the nanopore, the exterior boundary of the bulk solution in the model was extended to a distance ~100 μm from the opening of the GNM. The particle concentration was set at the nanopore orifice equal the concentration used in the experiment (2.2×10^{-8} mol·m^{-3}). A built-in function of the COMSOL software (Piecewise) was input to control the pressure applied at the pore orifice. We have previously demonstrated that 77% of the overall applied pressure drop occurs within the interior of a conical-shaped nanopore, the remaining pressure drop occurring in the external solution near the pore orifice.[33] Thus, in the simulation, the applied pressure was adjusted correspondingly to the 77% value of the experimental pressure. However, this adjustment does not significantly affect the probability curves presented below since the effect is canceled out with the application of both positive and negative pressures during the simulation. The boundary conditions and the mesh used in the study are summarized in Figure SI1. Strict time stepping (0.02 s) was employed in the COMSOL solver in order to fully resolve the multiple particle capture and release process.

Figure 5 shows the simulated particle concentration distribution inside the GNM at different times when the pressure waveform was applied. Initially (t = 0 s), no particles were present inside the GNM. At t > 0 s, a negative pressure was applied and the particles began to translocate through the opening of the GNM and continued to disperse into the pore with increasing time (t = 5 and 10 s). After the pressure was reversed at t ~ 12 s (corresponding to the experimental pressure waveform used in collecting the data in Figure 4), the particle concentration within the nanopore decreased due to the change of flow direction (t = 15, 20, and 25 s). With the continuing application of positive pressure (t = 50 s, simulation not shown), all of the particles that initially entered the pore have returned to the external solution.

The particle transfer rate (particles·s^{-1}) through the GNM was then computed by the integration of simulated particle flux across the GNM orifice as a function of time, and the results are shown as the solid curve in Figure 4b. Integration across the cross sectional area at a distance z = 50 nm inside the nanopore was used to calculate the particle flux through the GNM.

Dividing the instantaneous release transfer rate (Figure 4b) by the total number of capture translocations yields the particle release probability. Figure 6 shows the release probability histograms for different release pressures. Each bar represents the translocation probability in a 1 s interval centered about the corresponding time. The simulation-based curves are in good agreement with the experimental histograms.

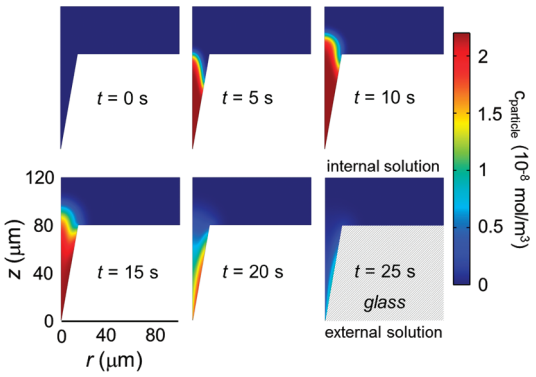

Figure 5. Simulated time-dependent particle concentration distribution within a 210 nm radius pore during a capture and release experiment. The particle concentration at the pore orifice was set as constant (2.2×10^{-8} mol/m^3). The particles were treated as points in this continuum simulation; *i.e.*, the finite size of the particle was not taken into account in the simulation. The −10 mmHg pressure was applied for the first ~12 s to drive particles from external solution to the pore interior (geometry shown in each figure), and then the pressure was reversed to 10 mmHg to drive particles back to the external solution. The simulation corresponds to the capture and release of 323 particles.

As shown in Figure 6, the histograms of release times depend strongly on the release pressure, with shorter release times at higher pressures.

The cumulative count percentages of particle release as a function of release time are plotted in Figure SI2. The release pressure has a strong effect on the overall release success rate at different times. Approximately 95% of the particles were released in 10 s after the pressure reversal at a release pressure of 20 mmHg. At 15 and 5 mmHg, that value decreased to 90 and 50%, respectively.

Capturing and Releasing Single Nanoparticles. The above experiments demonstrate that hundreds of particles may be captured and released in a single experiment, and that this process is well described by a convective diffusion model. Conversely, a single nanoparticle may be captured and released multiple times in an individual experiment.

Figure 7 shows an example of this experiment, in which a 120 nm radius particle was driven through a 210 nm radius nanopore at a pressure of −5 mmHg. The experiment was conducted in 0.1 M KCl solutions with low particle concentration (~10^7 particles/mL) and low pressure (5 mmHg) in order to capture only one particle in the programmed time. After a particle passed through the pore, the pressure was maintained at −5 mmHg for a time, τ, between 3 and 10 s, and then reversed to 5 mmHg to drive the particle back through the nanopore orifice. As shown in Figure 7a, for example, a particle translocating the pore in the capture direction was detected by an ionic current blockage. A time of ~6.5 s was allowed to elapse, and then the pressure was reversed, and the particle translocated the pore in the reverse direction, as evidenced by a second current blockage, indicating that the

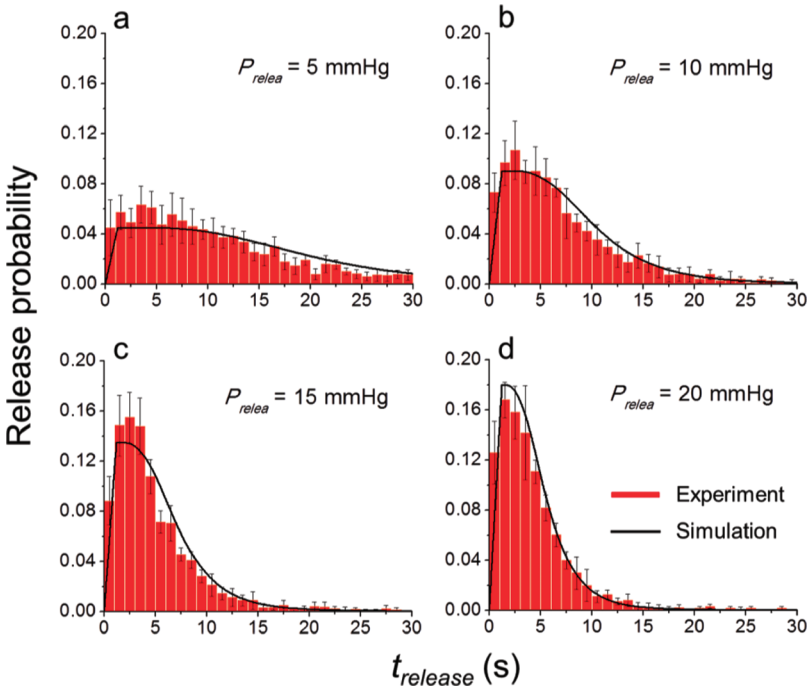

Figure 6. Release probabilities as a function of time for 120 nm radius particles from a 210 nm radius nanopore at release pressures of (a) 5, (b) 10, (c) 15, and (d) 20 mmHg. The capture pressure was −10 mmHg for all experiments. The particles were driven from the external solution into the GNM for ∼12 s; $t_{release}$ = 0 s in the figures corresponds to the instant at which pressure was reversed. The experimental data correspond to the capture and release of an average number of ∼370 particles.

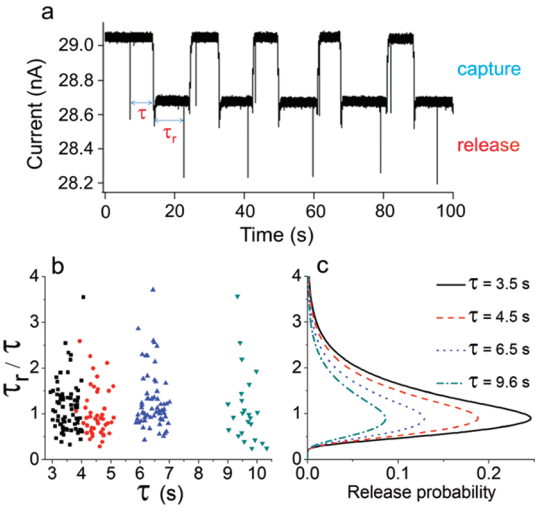

Figure 7. (a) Recording of *i*−*t* for capturing and releasing *single* 120 nm radius particle multiple times using a 210 nm radius GNM in a 0.1 M KCl solution containing 1.3 × 10^7 PS particles/mL. In this particular *i*−*t* trace, the particle was captured for τ = 6.5 ± 0.3 s at −5 mmHg and then released at +5 mmHg. V_{app}: 200 mV internal *vs* external. (b) Experimental τ_r/τ ratio distributions for different capture times, τ; τ_r refers to the time needed to release a single 120 nm radius particle. In each capture/release event, the particle was captured for τ = 3.5 ± 0.3 s (black squares, 74 events), τ = 4.5 ± 0.3 s (red circles, 49 events), τ = 6.5 ± 0.3 s (blue upward triangles, 65 events), and τ = 9.6 ± 0.3 s (green downward triangles, 24 events). (c) Simulated release probability curves as a function of τ_r/τ for different τ.

nanoparticle had entered the bulk solution. The pressure was then returned to −5 mmHg, driving the same particle back (or a different one) through the pore. We found that probability of releasing the particle was greater than 90%, as long as the time interval between the particle capture and the pressure reversal was less than 10 s. From the *i*−*t* trace, it is not possible to unequivocally state that the same particle is recaptured from the bulk solution after each release event. Because a large fraction of particles are recaptured immediately following the pressure reversal, we speculate that same particle is involved in the repeated capture/release pressure cycle. In addition, the finding that only a single particle is captured in each pressure cycle suggests that the same particle is captured and released multiple times during the experiment. However, whether or not the same particle is captured repeatedly from the bulk solution does not affect the single particle analysis presented below since the particles are all nominally the same size.

We varied the time between the capture translocation and the pressure reversal, τ, and measured τ_r, the time until the particle re-enters the external solution after pressure reversal, in order to probe the diffusional behavior of the particles that traveled different distances within the nanopore. Figure 7b shows the experimental distribution of the ratio τ_r/τ as a function of τ. These data were collected by capturing the nanoparticle for τ between 3.5 and 9.6 s. The spread in the experimental values of τ is due to the manual control of the pressure; however, precise values of both τ and τ_r are readily obtained from electrical signatures in the *i*−*t* curves. Figure 7b shows that the τ_r is strongly dependent on the elapsed time after the capture translocation, but

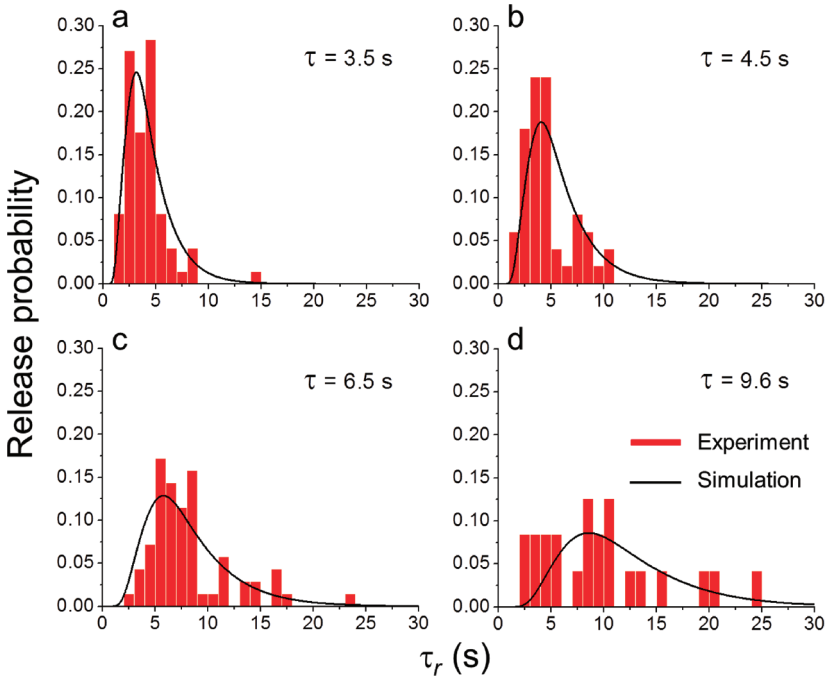

Figure 8. Experimental histograms of the probability of particle release as a function of release time (τ_r) at different capture times (τ), for the same data and experimental conditions described in Figure 7: (a) 3.5 s (74 events), (b) 4.5 s (49 events), (c) 6.5 s (65 events), and (d) 9.6 s (24 events). Simulated release probability curves are shown for comparison with the experimental data.

the distribution of ratios between the release time (τ_r) and capture time (τ) remains relatively constant.

In order to simulate the single-nanoparticle release probability (Figure 8), a particle flux pulse was generated manually in the simulations by setting the particle concentration at the orifice to 1.3×10^{-4} mol·m^{-3} and applying a low pressure (-3.75×10^{-2} mmHg) for a short time period (0.001 s). Since the time duration of the low-pressure pulse is very short, the particles move a very short distance into the pore (~200 nm). The number of particles driven into the pore during this pulse is of the order of unity (~1), as computed from the simulated particle concentration distribution. The resulting particle concentration distribution at t = 0.001 s was then used to simulate experiments where a single particle enters the pore (the capture event), transported deep into the pore (tens of micrometers), and then, following pressure reversal, is transported in the reverse direction until it passes again through the pore orifice. Following the introduction of the particle, the inflow concentration was set to 0 mol·m^{-3} such that the simulation modeled the capture of a single particle. The pressure was set to −5 mmHg, corresponding to the experimental pressure that drives the particle into the nanopore. The time step was adjusted to 2×10^{-5} s during the initial 0.004 s of "particle injection" and then increased to 0.001 and 0.02 s afterward. The particle probability distribution inside the GNM evolves with time due to pressure-driven flow and diffusion. After a predetermined time, the pressure was reversed. The moment at which the pressure was reversed corresponds to τ_r = 0 s (the origin of Figure 8). As τ increases, the maximum in the release probability distributions decreases, a consequence of diffusional broadening of the particle's position. The discrepancy between experiments and simulation originates primarily from the limited sample size, uncertainties in small pressures, as well as the assumptions and treatment in the simulation mentioned above. A discussion of the sources of error is presented in the Supporting Information.

The convection−diffusion model described above also successfully predicts the normalized distribution of τ_r/τ for single nanoparticle release, as shown in Figure 7c. Each release probability distribution curve has a maximum value at $\tau_r/\tau \sim 1$, in agreement with the experimental results.

Because the width of the τ_r/τ distribution curve (Figure 7c) is a function of the particle diffusion coefficient (D) (eq 4), the method presented above can be used, in principle, to measure the size of a single particle (indeed, in the absence of knowing the radii of the PS particles, the above analyses could have been performed by adjusting D in the simulations to obtain a "best fit" to the experimental data, and then using eq 2 to compute the particle size). For very small particles (<10 nm), manual control of the pressure reversal (1−2 s reversal time) may not be suitable since the particle may diffuse too quickly for accurate measurements. For instance, Gershow and Golovchenko employed a $\tau < 50$ ms to probe the diffusional property of DNA.[24] A systematic study is required to achieve a thorough understanding of this pressure capture and

release method and future applications. However, this problem can be potentially overcome by improved engineering design, such as using an automatic translocation signal-activated pressure reversal trigger.

CONCLUSIONS

A pressure-reversal method to capture and release nanoparticles using conical-shaped nanopores has been presented. An individual nanoparticle may be driven multiples times through a nanoscale orifice in a membrane to study stochastic diffusional broadening, or multiple particles may be driven through the orifice, and their sequence read out in the release translocations. Quantitative analysis of the capture and release events are in good agreement with predictions from finite-element simulations based on a convective diffusion model.

The pressure-reversal, resistive-pulse technique has several potential applications that expand analyses of nanoparticles. For instance, as noted above, it is possible to measure the size of a single particle by passing it repeatedly back and forth through the nanopore orifice and measuring the diffusional broadening reflected in the distribution of τ_r. In addition, it should be possible to study time-dependent reactions that change the particle size as the particle passes repeatedly between the external and internal solutions. A prerequisite for the study of time-dependent reactions is that the reaction must take place in a relatively short period of time in order to be detected in the release stage. These potential applications of the pressure-reversal, resistive-pulse method are currently under investigation.

METHODS

Chemicals. KCl, K_2HPO_4, KH_2PO_4 (Mallinckrodt), Triton X-100 (Sigma-Aldrich), 3-cyanopropyldimethylchlorosilane ($Cl(Me)_2Si(CH_2)_3CN$), and *n*-butyldimethylchlorosilane ($Cl(Me)_2Si(CH_2)_3CH_3$) (Gelest Inc.) were used as received. All aqueous solutions were prepared using water (18 MΩ·cm) from a Barnstead E-pure water purification system. The KCl solutions and phosphate buffered KCl solutions at a pH of 7.4 were made by dissolving appropriate amounts of each salt in ultrapure water. Acetonitrile (HPLC grade, J.T. Baker) was stored over 3 Å molecular sieves. Nonfunctionalized (120 nm radius, PS02N Lot 5708, Bangs Laboratories, Fishers, IN) and −COOH modified (160 nm radius, PC02N Lot 9172) polystyrene (PS) nanoparticles were dispersed in buffered KCl solutions as received.

Glass Nanopore Membrane (GNM) Fabrication and Surface Modification. GNMs were fabricated according to previous reports from our laboratory.[28] Briefly, an electrochemically sharpened Pt tip was sealed in a glass capillary (Dagan Corp., Prism glass capillaries, SB16, 1.65 mm outer diameter, 0.75 mm inner diameter, softening point 700 °C) using a H_2/air flame. The capillary was polished until a Pt nanodisk was exposed, using a sensitive electrical continuity tester. The Pt nanodisk was then partially removed by electrochemical etching in a 20% $CaCl_2$ solution with 5.9 V ac voltage applied between the Pt nanodisk and a large Pt wire counter electrode, after which the remaining Pt wire was gently pulled from the glass to yield a conical-shaped nanopore. The interior and exterior glass surfaces of the GNMs were silanized with $Cl(Me)_2Si(CH_2)_3CN$ or $Cl(Me)_2Si(CH_2)_3CH_3$ by immersing the GNM for 20 h in an acetonitrile solution containing the silane. The radius of the small orifice of the GNM, *a*, was determined from the ionic resistance of the pore in a 1.0 M KCl solution as previously described.[37] The relative uncertainty in *a* is estimated to be ∼10%. Optical microscopy was used to measure the thickness of the glass membrane (∼80 μm) containing the nanopore (Figure 2). All data reported herein were obtained with the single nanopore shown in Figure 2, which has an orifice radius of 210 nm. However, the capture and release data presented have been reproduced using numerous GNMs with orifice radii ranging from approximately 200 to 500 nm. Clogging of the nanopore occurs occasionally in the experiments, especially under high pressures with large volumetric flow rate. Particle aggregates are removed by rinsing the external and internal surfaces with H_2O. Gentle sonication of the GNM in H_2O or ethanol is also useful in removing particle aggregates, but care must be taken not to damage the pores.

Cell Configuration and Data Acquisition. A Pine RDE 3 potentiostat and a Dagan Cornerstone Chem-Clamp potentiostat was interfaced to a computer through a PCI 6251 data acquisition board (National Instruments). Current−time (*i*−*t*) curves were recorded by in-house virtual instrumentation written in LabVIEW (National Instruments) at a sampling frequency of 100 kHz. A 3-pole Bessel low-pass filter was applied at a cutoff frequency of 10 kHz. The GNM was filled and immersed in a 0.1 M KCl solution (pH 7.4, 0.1% Triton X-100), and polystyrene nanoparticles were homogeneously dispersed throughout the external solution. Electrical contact with the reservoirs was made using the Ag/AgCl electrodes and a voltage, V_{app}, applied between these electrodes to record *i*−*t* curves. The pressure across the GNM was applied using a 10 mL gastight syringe (Hamilton Co., Reno, NV) and was measured by a sphygmomanometer (pressure sensing range ∼−80 to 200 mmHg). The pressure unit (mmHg) used throughout this article is equivalent to 1 Torr or 1/760 of atmospheric pressure at room temperature. The sign of the pressure is defined as the pressure inside the capillary *versus* the external solution (which is at atmospheric pressure). Particles placed in the external solution are driven toward and through the pore at −*P*.

Computational Analysis and Finite-Element Simulations. The *i*−*t* recordings were plotted with Igor Pro software 6.0.2.4 (WaveMetrics, Lake Oswego, USA). The current pulses were detected and analyzed by QuB software package 1.5.0.20 (State University of New York at Buffalo, available at www.qub.buffalo.edu/). Statistical analyses of *i*−*t* recordings were accomplished by analyzing three or more segments of the data at each experimental condition. The finite-element simulations were performed with COMSOL Multiphysics 4.1 (Comsol, Inc.) on a high-performance desktop computer (16 GB RAM).

Acknowledgment. H.S.W. acknowledges financial support from the National Science Foundation. W.J.L. is grateful to Dr. H. Hu (University of Utah) for his assistance in modeling. The authors thank Dr. G. Barrall (Electronic BioSciences, San Diego) for helpful discussions.

Supporting Information Available: Details of the finite-element simulation, cumulative probability for multiple-particle release at different pressures, discussion of sources of error, and particle capture at different capture pressures. This material is available free of charge *via* the Internet at http://pubs.acs.org.

REFERENCES AND NOTES

1. Coulter, W. H. Means for Counting Particles Suspended in a Fluid. U.S. Patent 2,656,508, 1953.
2. Bayley, H.; Martin, C. R. Resistive-Pulse Sensing—From Microbes to Molecules. *Chem. Rev.* **2000**, *100*, 2575–2594.

3. Li, J.; Stein, D.; McMullan, C.; Branton, D.; Aziz, M. J.; Golovchenko, J. A. Ion-Beam Sculpting at Nanometre Length Scales. *Nature* **2001**, *412*, 166–169.
4. Chen, P.; Mitsui, T.; Farmer, D. B.; Golovchenko, J.; Gordon, R. G.; Branton, D. Atomic Layer Deposition to Fine-Tune the Surface Properties and Diameters of Fabricated Nanopores. *Nano Lett.* **2004**, *4*, 1333–1337.
5. Dekker, C. Solid-State Nanopores. *Nat. Nanotechnol.* **2007**, *2*, 209–215.
6. Martin, C. R.; Siwy, Z. S. Learning Nature's Way: Biosensing with Synthetic Nanopores. *Science* **2007**, *317*, 331–332.
7. Saleh, O. A.; Sohn, L. L. Direct Detection of Antibody–Antigen Binding Using an On-Chip Artificial Pore. *Proc. Natl. Acad. Sci. U.S.A.* **2003**, *100*, 820–824.
8. Bezrukov, S. M.; Vodyanoy, I.; Parsegian, V. A. Counting Polymers Moving through a Single Ion Channel. *Nature* **1994**, *370*, 279–281.
9. Kasianowicz, J. J.; Brandin, E.; Branton, D.; Deamer, D. W. Characterization of Individual Polynucleotide Molecules Using a Membrane Channel. *Proc. Natl. Acad. Sci. U.S.A.* **1996**, *93*, 13770–13773.
10. Gu, L. Q.; Braha, O.; Conlan, S.; Cheley, S.; Bayley, H. Stochastic Sensing of Organic Analytes by a Pore-Forming Protein Containing a Molecular Adapter. *Nature* **1999**, *398*, 686–690.
11. Bayley, H.; Cremer, P. S. Stochastic Sensors Inspired by Biology. *Nature* **2001**, *413*, 226–230.
12. Meller, A.; Nivon, L.; Branton, D. Voltage-Driven DNA Translocations through a Nanopore. *Phys. Rev. Lett.* **2001**, *86*, 3435–3438.
13. Henrickson, S. E.; Misakian, M.; Robertson, B.; Kasianowicz, J. J. Driven DNA Transport into an Asymmetric Nanometer-Scale Pore. *Phys. Rev. Lett.* **2000**, *85*, 3057–3060.
14. Zhou, K.; Li, L.; Tan, Z.; Zlotnick, A.; Jacobson, S. C. Characterization of Hepatitis B Virus Capsids by Resistive-Pulse Sensing. *J. Am. Chem. Soc.* **2011**, *133*, 1618–1621.
15. Sun, L.; Crooks, R. M. Single Carbon Nanotube Membranes: A Well-Defined Model for Studying Mass Transport through Nanoporous Materials. *J. Am. Chem. Soc.* **2000**, *122*, 12340–12345.
16. Ito, T.; Sun, L.; Crooks, R. M. Simultaneous Determination of the Size and Surface Charge of Individual Nanoparticles Using a Carbon Nanotube-Based Coulter Counter. *Anal. Chem.* **2003**, *75*, 2399–2406.
17. Ito, T.; Sun, L.; Bevan, M. A.; Crooks, R. M. Comparison of Nanoparticle Size and Electrophoretic Mobility Measurements Using a Carbon-Nanotube-Based Coulter Counter, Dynamic Light Scattering, Transmission Electron Microscopy, and Phase Analysis Light Scattering. *Langmuir* **2004**, *20*, 6940–6945.
18. Fraikin, J.-L.; Teesalu, T.; McKenney, C. M.; Ruoslahti, E.; Cleland, A. N. A High-Throughput Label-Free Nanoparticle Analyser. *Nat. Nanotechnol.* **2011**, *6*, 308–313.
19. Li, J. L.; Gershow, M.; Stein, D.; Brandin, E.; Golovchenko, J. A. DNA Molecules and Configurations in a Solid-State Nanopore Microscope. *Nat. Mater.* **2003**, *2*, 611–615.
20. Han, A.; Schürmann, G.; Mondin, G.; Bitterli, R. A.; Hegelbach, N. G.; de Rooij, N. F.; Staufer, U. Sensing Protein Molecules Using Nanofabricated Pores. *Appl. Phys. Lett.* **2006**, *88*, 093901.
21. Storm, A. J.; Storm, C.; Chen, J.; Zandbergen, H.; Joanny, J.-F.; Dekker, C. Fast DNA Translocation through a Solid-State Nanopore. *Nano Lett.* **2005**, *5*, 1193–1197.
22. Berge, L. I.; Feder, J.; Jossang, T. A Novel Method To Study Single-Particle Dynamics by the Resistive Pulse Technique. *Rev. Sci. Instrum.* **1989**, *60*, 2756–2763.
23. Berge, L. I.; Jossang, T.; Feder, J. Off-Axis Response for Particles Passing through Long Apertures in Coulter-Type Counters. *Meas. Sci. Technol.* **1990**, *1*, 471–474.
24. Gershow, M.; Golovchenko, J. A. Recapturing and Trapping Single Molecules with a Solid-State Nanopore. *Nat. Nanotechnol.* **2007**, *2*, 775–779.
25. Stein, D. Molecular Ping-Pong. *Nat. Nanotechnol.* **2007**, *2*, 741–742.
26. Bates, M.; Burns, M.; Meller, A. Dynamics of DNA Molecules in a Membrane Channel Probed by Active Control Techniques. *Biophys. J.* **2003**, *84*, 2366–2372.
27. Lathrop, D. K.; Ervin, E. N.; Barrall, G. A.; Keehan, M. G.; Kawano, R.; Krupka, M. A.; White, H. S.; Hibbs, A. H. Monitoring the Escape of DNA from a Nanopore Using an Alternating Current Signal. *J. Am. Chem. Soc.* **2010**, *132*, 1878–1885.
28. Zhang, B.; Galusha, J.; Shiozawa, P. G.; Wang, G.; Bergren, A. J.; Jones, R. M.; White, R. J.; Ervin, E. N.; Cauley, C. C.; White, H. S. Bench-Top Method for Fabricating Glass-Sealed Nanodisk Electrodes, Glass Nanopore Electrodes, and Glass Nanopore Membranes of Controlled Size. *Anal. Chem.* **2007**, *79*, 4778–4787.
29. Schibel, A. E. P.; Edwards, T.; Kawano, R.; Lan, W. J.; White, H. S. Quartz Nanopore Membranes for Suspended Bilayer Ion Channel Recordings. *Anal. Chem.* **2010**, *82*, 7259–7266.
30. Lan, W. J.; Holden, D. A.; White, H. S. Pressure-Dependent Ion Current Rectification in Conical-Shaped Glass Nanopores. *J. Am. Chem. Soc.* **2011**, *133*, 13300–13303.
31. Holden, D. A.; Hendrickson, G. R.; Lan, W. J.; Lyon, L. A.; White, H. S. Electrical Signature of the Deformation and Dehydration of Microgels during Translocation through Nanopores. *Soft Matter* **2011**, *7*, 8035–8040.
32. Lan, W. J.; Holden, D. A.; Zhang, B.; White, H. S. Nanoparticle Transport in Conical-Shaped Nanopores. *Anal. Chem.* **2011**, *83*, 3840–3847.
33. Lan, W. J.; Holden, D. A.; Liu, J.; White, H. S. Pressure-Driven Nanoparticle Transport across Glass Membranes Containing a Conical-Shaped Nanopore. *J. Phys. Chem. C* **2011**, *115*, 18445–18452.
34. Berg, H. C. *Random Walk in Biology*; Princeton University Press: Princeton, NJ, 1993.
35. White, R. J.; White, H. S. A Random Walk through Electron-Transfer Kinetics. *Anal. Chem.* **2005**, *77*, 214A–220A.
36. Einstein, A. Investigations on the Theory of the Brownian Movement. Edited by Fürth, R. *Ann. Phys.* **1905**, *17*, 549 (translated by Cowper, A. D.; Methuen: London, 1926).
37. White, R. J.; Zhang, B.; Daniel, S.; Tang, J. M.; Ervin, E. N.; Cremer, P. S.; White, H. S. Ionic Conductivity of the Aqueous Layer Separating a Lipid Bilayer Membrane and a Glass Support. *Langmuir* **2006**, *22*, 10777–10783.